ToF-SIMS study of oxide films thermally grown on nickel-base alloys

Xiaocui Wu, Svetlana Voyshnis, Antoine Seyeux, Yuriy Chumlyakov, Philippe Marcus

ToF-SIMS study of oxide films thermally grown on nickel-base alloys

Xiaocui Wu[a,b], Svetlana Voyshnis[b], Antoine Seyeux[b*], Yuriy Chumlyakov[c], Philippe Marcus[b*]

[a] Sino-French Institute of Nuclear Engineering and Technology, Sun Yat-sen University, Zhuhai 519082, China.

[b] PSL University, CNRS - Chimie ParisTech, Institut de Recherche de Chimie Paris, Physical Chemistry of Surfaces Group, 11 rue Pierre et Marie Curie, 75005 Paris, France

[c] Siberian Physical Technical Institute, Tomsk State University, Russia

* Corresponding authors e-mail: philippe.marcus@chimie-paristech.fr; antoine.seyeux@chimie-paristech.fr

Abstract: The oxidation behaviours of polycrystalline and monocrystalline Ni-base alloys (Ni-16Cr-8Fe (wt%)) were investigated *in situ* by Time-of-Flight Secondary Ion Mass Spectrometry (ToF-SIMS). The oxide layer formed is duplex: an inner chromium-rich layer and an outer layer which is rich in nickel and iron. Time evolution of the composition of inner layer from pure Cr_2O_3 towards spinel ($NiCr_2O_4$) was observed. The oxidation kinetics was accelerated by alloy grain boundaries, which can favour the diffusion of chromium. Both the parabolic and volatilization constants increased with increasing temperature, with k_p varying from 1.9×10^{-3} to 1.6×10^{-2} $nm^2.s^{-1}$, and k_v from 1.0×10^{-3} to 2.9×10^{-3} $nm.s^{-1}$.

Keywords: A. Nickel Alloy; B. ToF-SIMS; C. Oxidation kinetics

Introduction

Lifetime prediction of the PWR components, especially the steam generator (SG), is crucial for the development of nuclear industry. The SG is often made of nickel-based alloys (more specifically Alloy 600 or 690) which can be susceptible to stress corrosion cracking [1-11]. The release of corrosion products (such as Ni) in the solution will also lead to a significant increase in the radioactive contamination of the primary circuit via neutron activation of ^{57}Ni. The oxide film formed on the SG tube surfaces plays an important role in the limitation of SCC and slow-down of Ni release phenomena, since i) it is identified as a diffusion barrier and limits the release of Ni [12], and ii) the oxide film stability is a key parameter in SCC initiation. Thus the study of the oxidation of nickel-based alloy in primary coolant is of great importance for the safety of the PWR power plants.

Numerous studies have been carried out to investigate the oxidation of nickel-base alloys, and the results reveal that whatever oxidizing medium is employed, in particular in an aqueous medium at high temperature, the oxide layer formed is duplex. The inner layer is rich in chromium, adherent and compact, and the outer layer is rich in iron and nickel [13-29]. The latter may be

porous, and is composed of inhomogeneous crystals randomly distributed, or is simply composed of a layer of hydroxide. The composition of each layer varies according to the nature of the alloy under consideration as well as the temperature, pressure, and chemistry of the medium [4, 25, 30-34]. The inner layer is mainly composed of chromium oxide with more or less nickel and iron oxide to form a spinel (Ni, Fe)(Fe, Cr)$_2O_4$, or of simple Cr_2O_3 oxides with possible Ni-rich and/or Fe-rich islands. The outer layer consists of crystals which are rich in iron and nickel and is often characterized by a mixture of hydroxide, oxyhydroxide and nickel ferrite ($Ni_xFe_{3-x}O_4$).

In this study, oxide layers formed on Alloy 600 during early stages of oxidation were characterized *in situ* in the gaseous medium under low oxygen pressure, using advanced surface characterization technique, ToF-SIMS, and the oxidation kinetics at different temperatures was also monitored. The study of the first oxidation step is very important because the early oxidation stage governs to a large extent the subsequent evolution of the behaviour of materials when interacting with their environment. In addition, the thermally formed oxide is a good model for oxides formed in high temperature water.

Material and methods

In this study, two types of NiCrFe alloys were used. One is a polycrystalline cast Alloy 600 (Ni-16Cr-9Fe (wt%), referenced WF675), provided by the company Imphy. This is the material used for the fabrication of steam generators of PWR power plants. Another is monocrystalline (111) Alloy 600 (Ni-16Cr-8Fe (wt%)), grown by the Bridgman method. The samples are plates with a surface area of 1.1×1.1 cm^2 and thickness of 1 mm.

The oxidation kinetics of polycrystalline and monocrystalline Ni alloys was investigated *in situ* in the main chamber of a ToF-SIMS V spectrometer (ION-TOF GmbH, Muenster, Germany). This chamber is pumped continuously to keep an ultra-high vacuum (UHV), in which the normal pressure is inferior to 5×10^{-9} mbar. The samples were mechanically polished to a ¼ µm diamond finish and then transferred to the main chamber. An Ar^+ sputtering was performed over a 1 mm^2 area at 2 keV in order to remove the native oxide initially formed on the sample surface. Then an annealing at 400℃ was elaborated during 1 h, followed by a new Ar^+ sputtering. Finally, another 1h was required for vacuum pumping until a residual pressure below 10^{-8} mbar is reached in the main chamber.

O_2 was then introduced in the main chamber through a leak valve, and the oxygen partial pressure was maintained at 1.2×10^{-6} mbar. A 1.6 pA Bi^+ analysis beam was used to scan an area of 30 x 30 µm^2. For ToF-SIMS depth profiling, a dual-beam mode was used by alternating the analysis process with a sputtering step. The etching sequence was carried out using a 10 nA (500 eV) Cs^+ ion beam for oxidation at 250℃ and a 20 nA (500 eV) Cs^+ ion beam for that at 350℃, rastered over an area of 150×150 µm^2. Because of sample surface destruction, every measurement was performed at a different and new point on the 1 mm^2 area that has been cleaned at the beginning of the experiment [35].

ToF-SIMS depth profiles were carried out regularly at oxidation time of 0 min, 1 min, 5 min, 15 min, 30 min, 1 h, 1 h 30 min,… until a stationary regime was reached (with a stable oxide film thickness). The intensity in the profiles is usually plotted as a function of sputtering time. The transformation to oxide layer thickness was performed by a mechanical profilometer (Dektak 150, Veeco, Veeco-Instrument Europe, Dourdan, France), which gives sputtering rates of 0.055 nm.s^{-1}

and 0.11 nm.s^{-1} for oxidation at 250℃ and 350℃, respectively. We assume that the sputtering rates are constant, and do not change with oxidation time.

Results and discussion

According to the ToF-SIMS study performed on a thermally oxidized model sample Ni-30Cr (wt%), Mazenc et al. [36] showed that the CrO^- ion is mainly a marker for the presence of chromium oxide (Cr_2O_3). However, the CrO_2^- ion may correspond to several compounds. This signal is more intense in nickel chromite ($NiCr_2O_4$) than in chromium oxide. It is therefore not specific to a single compound but is representative of the two species. Thus, $NiCr_2O_4$ is associated with the presence of a maximum on the $NiCrO^-$ signal and a maximum, or a shoulder on the CrO_2^- signal. The FeO^- and FeO_2^- ions are associated with iron oxide, and NiO_2^- is associated with nickel oxide. The Ni_2^- ion is used to locate the position of the metal/oxide (M/O) interface. Indeed, this signal, characteristic of metallic nickel, will be extremely weak in the oxide and will reach a maximum intensity when the metallic substrate is reached.

Fig. 1 shows the ToF-SIMS profiles obtained on the polycrystalline Ni alloy at 250℃ for different oxidation times.

For the ToF-SIMS *in situ* oxidation experiment, the sample was prepared under UHV in order to remove the native oxide and thus to obtain a metallic surface (there is less than a monolayer of oxide after *in situ* surface preparation). After 1 min of oxidation, we start to see the stratification of the oxide layer, as shown in Fig. 1(a). The obtained ToF-SIMS profiles can be separated into three regions: the first one between 0 and 2 s, although difficult to precisely interpret because of the establishment of the stationary regime, is characterized by intense ion signals of FeO_2^- and NiO_2^-. Then, a second region is characterized by a marked decrease of the intensity of FeO_2^- signal and intense CrO_2^- and CrO^- signals, the latter reaches its maximum intensity after approximately 4 s. Finally, as one probes deeper in the material, a slow decrease in the intensity of characteristic signals of the oxides (MO_2^-, MO^-, O^-) associated with the progressive enhancement of the Ni_2^- signal which reaches its maximum intensity after 15 s of sputtering, i.e. ~ 0.8 nm, indicate here the position of the M/O interface. Moreover, the $NiCrO^-$ signal increases within the second region, and reaches a maximum intensity after approximately 9 s of etching, i.e. before the M/O interface, indicating the formation of $NiCr_2O_4$ in the inner oxide layer near the M/O interface. The formation of spinel beneath the chromium oxide requires a prior Ni enrichment (hence Cr depletion) in the alloy near the M/O interface. This is indeed observed in the Ni^{2-} depth profiles on the polycrystalline alloy.

By applying the same analysis approach, we can conclude that after 15 min of oxidation, as shown in Fig. 1(b), the oxide layer formed is still duplex: an inner layer of Cr_2O_3 with the presence of $NiCr_2O_4$, and a mixed outer layer consisting of iron oxide and nickel oxide. However, from this time a shoulder begins to appear on the FeO_2^- signal at about 7 s, which means that in the inner oxide layer there is $NiCr_2O_4$ containing iron. The M/O interface is reached after 25 s of etching, i.e. 1.4 nm.

Oxygen continues to be introduced into the main chamber. After 2 h 30 min of oxidation, the outer layer, extending from 0 to 4 s, remains thin and is rich in iron and nickel. While the inner layer continues to grow over time until a stationary regime was reached, and is rich in chromium. The Ni_2^- signal reaches its maximum intensity after 34 s of etching, i.e. 1.9 nm, indicating here the

position of the M/O interface.

From the above analysis, we can see that the growth of the oxide layer is mainly associated to the growth of the inner oxide layer, while the outer layer remains very thin, and its thickness is almost unchanged. Normally, given a chromium-rich inner layer, it is supposed to be corrosion resistant.

After reaching the metallic substrate a quasi-plateau can be observed on the characteristic oxide signals, which may be assigned to the reoxidation of the alloy when the metal surface is reached. The depth profiles are obtained *in situ* during the oxidation experiment, with an oxidation rate equal to the sputtering rate of the ToF-SIMS Cs^+ gun.

The oxidation kinetics was also performed on polycrystalline Alloy 600 at 350℃, and the results are shown in Fig. 2.

According to the same analysis, we can conclude that the oxide layer formed on the polycrystalline Ni alloy during oxidation in the gaseous medium under low oxygen pressure at 350℃ is duplex. The nature of the oxides composing the outer layer remains unchanged whatever the oxidation time, and its thickness remains also almost constant (~ 0.3 nm, of the order of a monolayer). The outer layer is composed of a mixture of iron oxide and nickel oxide. The inner layer contributes mainly to the growth of the oxide layer, of which the composition changes with oxidation time. It is mainly composed of chromium oxide for short oxidation time (up to about 15 min), then, $NiCr_2O_4$ containing some iron oxides ($Ni_{1-x}Fe_xCr_2O_4$) begins to appear in the inner layer near the M/O interface. As indicated above in Fig. 1, beyond the M/O interface, the nearly constant signals of the characteristic oxides are assigned to reoxidation of the reactive metal surface that is still exposed to oxygen in the *in situ* oxidation procedure. As the ToF-SIMS profiles demonstrated the initial formation of Cr_2O_3 and the later formation of $NiCr_2O_4$, there is necessarily an intermediate stage of nucleation and growth of $NiCr_2O_4$. So we can conclude that $NiCr_2O_4$ appears in the inner layer in the form of islands.

In order to avoid the possible influence of grain boundaries on the oxidation of the Ni alloy, and possibly to observe the effect of grain boundaries on the oxidation behaviours, *in situ* oxidation was performed on a monocrystalline (111) oriented Ni alloy (Ni-16Cr-8Fe, wt%). The experimental conditions are exactly the same as that used for the polycrystalline alloy oxidized at 350℃ previously, and the results are given in Fig. 3.

The same analysis of the ToF-SIMS profiles reveals that the oxide layer formed on the monocrystalline (111) Ni alloy is duplex, and its nature and composition remain unchanged with oxidation time. The inner layer is mainly composed of Cr_2O_3, and the outer layer is a mixture of iron and nickel oxide. In addition, the thickness of the outer layer is almost constant, and the inner layer contributes mainly to the growth of the oxide film.

However, we can notice that after 30 min of oxidation, shoulders can be observed on the CrO_2^- and CrO^- signals near, but after the M/O interface, while there is no maximum associated on the $NiCrO^-$ signal, so there is no spinel in the inner oxide. These shoulders may then be assigned to a rapid reoxidation of the M/O interface, which is faster than the sputtering rate of the ToF-SIMS Cs^+ gun. As indicated above, since the oxygen pressure was maintained at a constant level for oxidation *in situ*, during the process of ion sputtering, the alloy surface can be reoxidized. The oxidation kinetics of monocrystalline Ni alloy is slower than that for the polycrystalline sample (see Fig. 5), so more chromium will accumulate in the metallic substrate near the M/O interface (in Alloy 600, the oxidation of chromium is faster than that of nickel and iron), and thus

resulting in a reoxidation process faster than the etching process, which explains the presence of shoulders on the CrO_2^- and CrO^- signals in the ToF-SIMS profiles.

For the polycrystalline alloy, this phenomenon was not observed, and this is attributed to the presence of grain boundaries which act as fast diffusion paths. The rapid oxidation of the sample surface results in a depletion of chromium under the oxide layer. So the sputtering rate becomes faster than the reoxidation process and thus no shoulders are observed on the CrO_2^- and CrO^- signals when the M/O interface is overpassed. In addition, the accumulation of Ni in the metallic substrate near the M/O interface facilitates the formation of spinel in the inner oxide layer. However, for the monocrystalline alloy, there is no strong chromium depletion, and the inner layer remains mainly composed of chromium oxide. The evolution of the composition of the oxide layer formed on polycrystalline and monocrystalline alloy 600 is shown more explicitly in Fig. 4.

The thickness of the oxide layer can be measured based on the ToF-SIMS profiles obtained at different oxidation times, thus we can determine the growth of the oxide layer formed on polycrystalline and monocrystalline Alloy 600 at different oxidation temperatures, and the results are compared with that obtained at 300℃ by Voyshnis, as shown in Fig. 5.

The kinetics of oxidation seems to follow a logarithmic-type law, which, according to previous work [35], can be explained by the competition between parabolic growth and oxide layer volatilization. From Fig. 5, two regions can be observed on each curve: a first region where the oxide layer grows rapidly, essentially because of the growth of the chromium-rich inner layer. Then the growth of the oxide layer seems to have reached a stationary regime (growth rate = volatilization rate), with an almost stable film thickness.

Moreover, we observe that the oxidation kinetics of the monocrystalline alloy sample is much slower than that of the polycrystalline alloy at the same temperature, while the stationary oxide layer thickness remains almost the same. The slower oxidation kinetics may be explained by the absence of grain boundaries for the single crystal, which act as fast diffusion paths and are favoured locations for oxidation to occur for polycrystals. In contrast, the stationary thickness may be governed by the diffusion in the oxide and the volatilization of chromium oxide. To clarify the effects of grain boundaries on the oxidation kinetics, it would be necessary to obtain depth profiles on grains and at grain boundaries, which was not done here.

Comparing the growth of oxide layer on the polycrystalline Ni alloy at different temperatures, we observe that the oxidation kinetics is faster with increasing temperature. This is the expected result since the diffusion process accelerates with increasing temperature, and the diffusion of the species in the oxide layer is the limiting step for the growth of oxide layers formed on this alloy. However, the oxide layer thickening is also limited by the evaporation of chromium oxide on this alloy, as shown in a previously published paper on the oxidation of chromium at 300℃ [35].

The oxidation kinetics can then be fitted by Eq. (1), as shown in the previous paper [35]:

$$t = \frac{k_p}{k_v^2}\left[-\frac{k_v}{k_p}x - \ln\left(1 - \frac{k_v}{k_p}x\right)\right] \quad (1)$$

where k_p is the parabolic constant, and k_v is the constant of volatilization.

The fittings of the curves are shown in Fig. 6, and the results calculated for the parabolic and volatilization constants are given in Table 1.

From Table 1 we can see that k_p (as expected) and k_v increase with increasing temperature. Standard errors of k_p and k_v are 10^{-4} $nm^2.s^{-1}$ and 10^{-4} $nm.s^{-1}$. Compared to the value of k_p calculated in [35] for the oxidation of chromium at 300°C, i.e. 1.9 x 10^{-2} $nm^2.s^{-1}$ at oxygen

pressure of 2.0 x 10^{-6} mbar, the oxidation kinetics of polycrystalline Ni alloy (solid line) is about three times slower, and this is due to the nature of the material and the differences in the composition of the oxide layer. The formation of spinel in the inner oxide layer (instead of pure chromium oxide [35]) may retard the oxidation of the alloy.

If we do the fitting only for the first few experimental points where the composition of the oxide is closer to pure chromium oxide (dashed line in Fig. 6), we find closer values of k_p and k_v compared to that calculated in [35], with a faster growth kinetics compared to the solid line. This difference is assigned to a lower diffusion coefficient of O^{2-} in the spinel than in pure Cr_2O_3. The diffusion coefficient of oxygen in chromium oxide can then be deduced by using the simplified Fick's law and Tedmon's equation, and the results are shown in Table 1. The diffusion coefficient is of the order of 10^{-17} $cm^2.s^{-1}$ at oxidation temperatures of 250℃ and 300℃, and of the order of 10^{-16} $cm^2.s^{-1}$ at an oxidation temperature of 350℃.

From the measurements of k_p at three different temperatures, one can calculate, assuming that k_p follows an Arrhenius behaviour ($k_p = k_{p_0} \exp\left(-\frac{E_A}{RT}\right)$), the activation energy of the parabolic constant. We found an activation energy of 58 ± 1 kJ/mol (0.60 ± 0.01 eV) for the oxidation of Ni alloy, and 72 ± 3 kJ/mol (0.74 ± 0.03 eV) for the oxidation of chromium (in the early oxidation stage). The values calculated appear to be smaller than that found in the literature, which are generally superior to100 kJ/mol [37-39].

Finally, we can compare the attenuation of the characteristic oxide signals, for example, the CrO^- signal, after the M/O interface on the ToF-SIMS profiles obtained for poly and monocrystalline alloy samples at different oxidation times (Fig. 7).

In this figure, the abscissa 0 indicates the position of the M/O interface. The intensity of the profiles was normalized compared to that at the M/O interface. From this figure, it appears that the characteristic CrO^- oxide signal in the ToF-SIMS profiles obtained for the monocrystalline alloy decreases slightly faster than that obtained for the polycrystalline alloy as we enter the metallic substrate. Although the effect of interface roughness cannot be excluded in this measurement, these different behaviours between polycrystalline and monocrystalline samples suggest the penetration of oxides into the metallic substrate through grain boundaries for oxidation of the polycrystalline alloy sample.

Conclusions

Oxide layers formed on polycrystalline and monocrystalline Ni-base alloys (Ni-16Cr-8Fe (wt%, Alloy 600) during early stages of oxidation were characterized *in situ* by ToF-SIMS, and the oxidation kinetics at different temperatures was measured.

The results show that the oxide layers formed on both polycrystalline and monocrystalline alloys are duplex, with a chromium-rich inner layer and an outer layer which is rich in nickel and iron. As regards the inner layer, at 350℃, it is mainly composed of chromium oxide at short oxidation time. At longer oxidation time, the inner layer contains more Ni and evolves from pure Cr_2O_3 towards a Cr_2O_3 layer containing islands of spinel for the polycrystalline alloy. This evolution is not observed for the oxidation of the monocrystalline alloy at similar temperature and for the same oxidation time where the composition of the inner layer remains close to Cr_2O_3. The temperature has also an influence on the composition of the oxide layer. For the polycrystalline

alloy oxidized at 250℃, the inner layer is composed of chromium oxide with the presence of islands of spinel from the first oxidation time. As regards the outer layer, it consists of NiO and Fe_2O_3 whatever the sample is.

In terms of the oxidation kinetics, the inner layer contributes mainly to the growth of the oxide layer, whereas the outer layer remains very thin, and its thickness is almost unchanged with oxidation time. However, the oxidation kinetics for the polycrystalline alloy is faster than that for the single crystal before the establishment of a stationary regime. This can be explained by the presence of grain boundaries in the polycrystal which act as fast diffusion paths and are favoured positions for oxidation to occur. A model was used to describe the kinetics taking into account the diffusion limited oxidation and volatilization of chromium oxide. The variation of the parabolic and volatilization constants, k_p and k_v, with the oxidation temperature was calculated, and they were found to increase with increasing temperature, with k_p varying from 1.9×10^{-3} to 1.6×10^{-2} $nm^2.s^{-1}$, and k_v varying from 1.0×10^{-3} to 2.9×10^{-3} $nm.s^{-1}$.

The comparison between polycrystalline and monocrystalline alloys shows the significant influence of grain boundaries on the oxidation of nickel-base alloys. The enrichment of nickel in the inner layer with the oxidation time is the result of the depletion of chromium in the metallic substrate due to its preferential oxidation at short exposure time. Thus, chromium oxide is preferentially formed on the alloy surface and in the grain boundaries of the substrate, which is then enriched in nickel. The nickel enrichment in the M/O interface is thought to be at the origin of the modification of the thermodynamic conditions at this interface, leading to the transformation of phases, after enough long oxidation time, from Cr_2O_3 to $NiCr_2O_4$. At lower temperature, i.e. 250℃, the diffusion of chromium from the metallic substrate to the M/O interface was slowed down, thus resulting in a more rapid depletion of chromium and the formation of chromium oxide with the presence of islands of spinel since the first oxidation time.

Acknowledgments

This work was support by Région Île-de-France for the ToF-SIMS equipment.

References

[1] R.W. Staehle, J.J. Royuela, T.L. Raredon, E. Serrate, C.R. Morin, R.V. Farrar, Effect of alloy composition on stress corrosion cracking of Fe-Cr-Ni base alloys, Corros. 26 (1970) 451-486.

[2] P.L. Andresen, Fracture mechanics data and modeling of environmental cracking of nickel-base alloys in high-temperature water, Corros. 47 (1991) 917-938.

[3] G. Sui, J.M. Titchmarsh, G.B. Heys, J. Congleton, Stress corrosion cracking of alloy 600 and alloy 690 in hydrogen/steam at 380°C, Corros. Sci. 39 (1997) 565-587.

[4] K. Arioka, T. Yamada, T. Terachi, R.W. Staehle, Intergranular stress corrosion cracking behavior of austenitic stainless steels in hydrogenated high-temperature water, Corros. 62 (2006) 74-83.

[5] P.L. Andresen, J. Hickling, A. Ahluwalia, J. Wilson, Effects of hydrogen on stress corrosion crack growth rate of nickel alloys in high-temperature water, Corros. 64 (2008) 707-720.

[6] P.L. Andresen, M.M. Morra, Stress corrosion cracking of stainless steels and nickel alloys in high-temperature water, Corros. 64 (2008) 15-29.

[7] M. Sennour, P. Laghoutaris, C. Guerre, R. Molins, Advanced TEM characterization of stress corrosion Cracking of alloy 600 in pressurized water reactor primary water environment, J. Nucl. Mater. 393 (2009) 254-266.

[8] R.B. Rebak, Stress corrosion cracking (SCC) of nickel-based alloys, in: V.S. Raja, T. Shoji (Eds.), Stress Corrosion Cracking: theory and practice, 1st ed., Woodhead Publishing, 2011, pp. 273-306.

[9] T. Terachi, T. Yamada, T. Miyamoto, K. Arioka, SCC growth behaviors of austenitic stainless steels in simulated PWR primary water, J. Nucl. Mater. 426 (2012) 59-70.

[10] K. Arioka, T. Yamada, T. Miyamoto, M. Aoki, Intergranular stress corrosion cracking growth behavior of Ni-Cr-Fe alloys in pressurized water reactor primary water, Corros. 70 (2014) 695-707.

[11] D. Feron, R.W. Staehle, Stress corrosion cracking of nickel based alloys in water-cooled nuclear reactors: the coriou effect, Woodhead Publishing, 2016.

[12] L. Guinard, O. Kerrec, D. Noel, S. Gardey, F. Coulet, Proc. of 7th international conference of water chemistry of nuclear reactor systems, BNES, Bournemouth, 1996.

[13] A.P. Bond, H.H. Uhlig, Corrosion behavior and passivity of nickel-chromium and cobalt-chromium alloys, J. Electrochem. Soc. 107 (1960) 488-493.

[14] N.S. Mcintyre, D.G. Zetaruk, D. Owen, XPS study of the initial growth of oxide films on Inconel 600 alloy. Appl. Surf. Sci. 2 (1978) 55-73.

[15] N.S. Mcintyre, D.G. Zetaruk, D. Owen, X-Ray photoelectron studies of the aqueous oxidation of Inconel 600 alloy. J. Electrochem. Soc. 126(1979) 750-760.

[16] M.E. Pick, Proc. of 3rd international conference of water chemistry of nuclear reactor systems, BNES, Bournemouth, 1983.

[17] A.L. Hanson, H.S. Issacs, H.W. Kraner, Determination of surface oxide compositions on Alloy 600 using nuclear analytical techniques. Corros. 41 (1985) 324-327.

[18] F. Carette, M.C. Lafont, G. Chataignier, L. Guinard, B. Pieraggi, Analysis and TEM examination of corrosion scales grown on Alloy 690 exposed to pressurized water at 325°C, Surf. Interface Anal. 34 (2002) 135-138.

[19] A. Machet, A. Galtayries, P. Marcus, P. Combrade, P. Jolivet, P. Scott, XPS Study of oxides formed on nickel-base alloys in high-temperature and high-pressure water, Surf. Interface Anal. 34 (2002) 197-200.

[20] A. Machet, A. Galtayries, S. Zanna, P. Marcus, XPS and STM study of the growth and structure of passive films in high temperature water on nickel-base alloy, Electrochim. Acta 49 (2004) 3957-3964.

[21] A. Machet, A. Galtayries, P. Marcus, Kinetics of passivation of a nickel-base alloy in high temperature water, in: D. Feron, J.-M. Olive (Eds.), Corrosion Issues in Light Water Reactors: Stress corrosion cracking, Woodhead Publishing, 2007, pp. 44-56.

[22] M. Sennour, L. Marchetti, F. Martin, S. Perrin, R. Molins, M. Pijolat, A detailed TEM and SEM study of Ni-base alloys oxide scales formed in primary conditions of pressurized water reactor, J. Nucl. Mater. 402 (2010) 147-156.

[23] H. Lefaix-Jeuland, L. Marchetti, S. Perrin, M. Pijolat, M. Sennour, R. Molins, Oxidation kinetics and mechanisms of Ni-base alloys in pressurized water reactor primary conditions: influence of subsurface defects, Corros. Sci. 53 (2011) 3914-3922.

[24] Z. Zhiming, W. Jianqiu, H. En-Hou, K. Wei, Analyses of surface oxide films on ground alloy 690TT afetr immersion for different times, Acta Metall. Sin. 47 (2011) 823-830.

[25] K. Arioka, T. Yamada, T. Miyamoto, T. Terachi, Dependence of stress corrosion cracking of alloy 690 on temperature, cold work, and carbide precipitation - role of diffusion of vacancies at crack tips, Corros. 67 (2011) 1-18.

[26] J. Caballero, C. Duhamel, T. Couvant, J. Crépin, Intergranular oxidation of alloy 600 exposed to simulated PWR primary water, Mat. Sci. 47 (2015).

[27] S. Fujimoto, W.S. Kim, M. Sato, J.Y. Son, M. Machida, K.T. Jung, H. Tsuchiya, Characterization of oxide films formed on alloy 600 and alloy 690 in simulated PWR primary water by using hard X-ray photoelectron spectroscopy, J. Solid State Electrochem. 19 (2015) 3521-3531.

[28] W. Feng, T.M. Devine, Corrosion behavior of inconel alloys of nuclear power steam generator tube in high-temperature and high-pressure water, Corros. Sci. Prot. Technol. 27 (2015) 19-24 (in chinese).

[29] W. Feng, T.M. Devine, Oxide films formed on Inconel 600 and Inconel 690 in simulated PWR primary water environment, Corros. Sci. Prot. Technol. 27 (2015) 339-344 (in chinese).

[30] D. Costa, P. Marcus, Modifications of passive films formed on Ni-Cr-Fe alloys with chromium content in the alloy and effect of adsorbed or segregated sulphur, in: P. Marcus, B. Baroux, M. Keddam (Eds.), Modifications of Passive Films, The Instituite of Materials, London, 1994, pp. 17-25.

[31] N.E. Hakiki, D. Colin, O.D. Bouvier, E. Picquenard, G. Sagon, et.al, Study of oxide films formed on nickel base alloys 600, 690 and 316L stainless steel in lithiated water, Proceedings of the International Symposium Fontevraud III 1 (1994) 327-336.

[32] N.S. Mcintyre, R.D. Davidson, T.L. Walzak, A.M. Brennenstühl, F. Gonzalez, S. Corazza, The corrosion of steam generator surfaces under typical secondary coolant conditions: effects of pH excursions on the alloy surface composition, Corros. Sci. 37 (1995) 1059-1083.

[33] L. Guinard, C. Gabet, T. Czerwiec, E. Riquelme, O. Kerrec, Effect of surface passivation of Inconel 690 on oxidation in primary circuit conditions, Water Chemistry of Nuclear Reactor Systems 8 (2000) 67-72.

[34] M. Dupin, P. Gosser, M.G. Walls, B. Rondot, J.-L. Pastol, S. Faty, M.G.S. Ferreira, M.D.C. Belo, Influence du pH sur les propriétés chimiques et structurales des films d'oxyde formés sur l'acier 316L et les alliages 600 et 690 dans les milieux aqueux à haute température, Ann. Chim. Sci. Mat. 27(2002) 19-32.

[35] C. Poulain, A. Seyeux, S. Voyshnis, P. Marcus, Volatilization and transport mechanisms during Cr oxidation at 300°C studied in situ by ToF-SIMS, Oxid. Met. 88 (2017) 423-433.

[36] A. Mazenc, A. Galtayries, A. Seyeux, P. Marcus, S. Leclercq, ToF-SIMS study of the behavior of thermally oxidized films formed on nickel-based 690 alloy in high-temperature water, Surf. Interface Anal. 45 (2013) 583-586.

[37] A. Moosa, J.K. Ahmed, A. Hoobi, Oxidation properties in CO_2 of Inconel alloy 600 coated by simultaneous aluminizing-chromizing process, Chin. J. Aeronautics 20 (2007) 134-139.

[38] C. Salmon, D. Tiberghien, R. Molins, C. Olin, F. Delannay, Oxidation behavior in air of thin

alloy 601 fibers, Mater. High Temp. 17 (2000) 271-278.
[39] F. Lebreau, M.M. Islam, B. Diawara, P. Marcus, Structural, magnetic, electronic, defect, and diffusion properties of Cr_2O_3: a DFT+U study, J. Phys. Chem. C 118 (2014) 18133-18145.

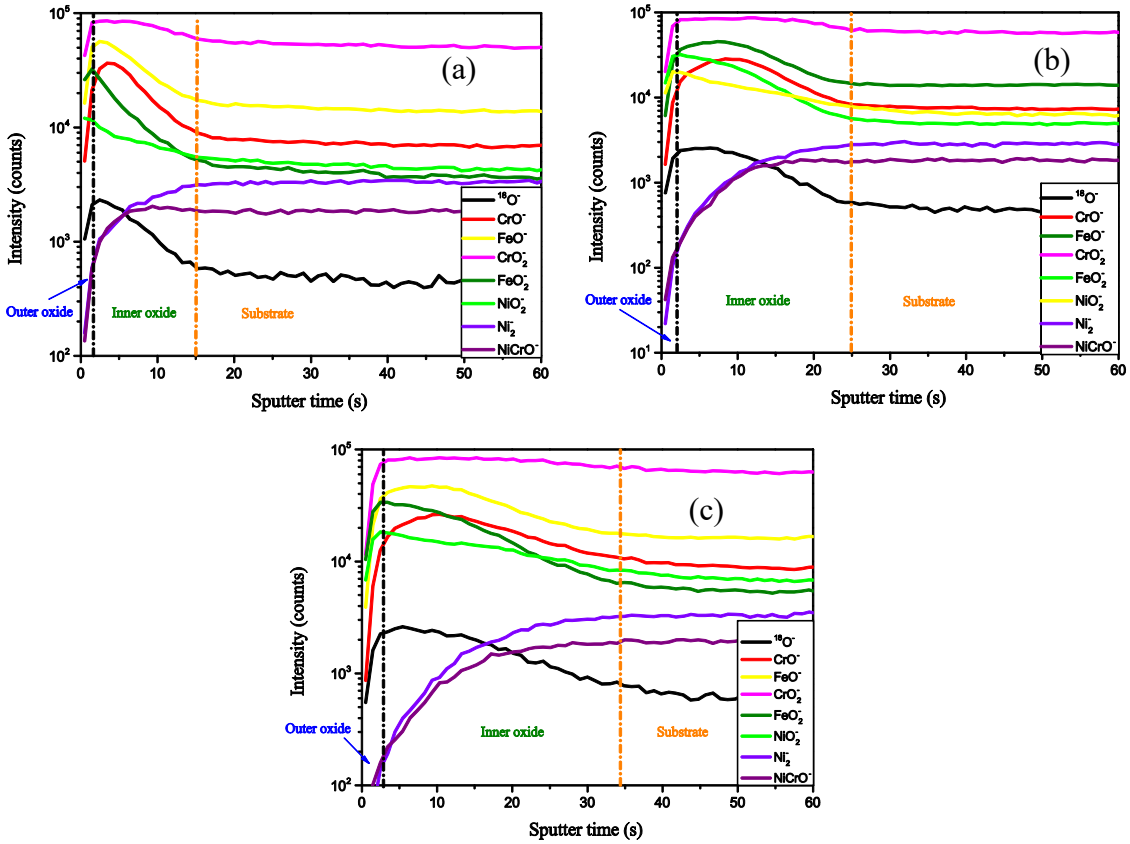

Fig. 1. ToF-SIMS profiles [Bi^+ 1.6 pA, 30×30 μm^2, Cs^+ 10 nA, 500 eV, 150×150 μm^2] obtained on the polycrystalline Ni alloy after oxidation at 250℃ for 1 min (a), 15 min (b) and 2 h 30 min (c).

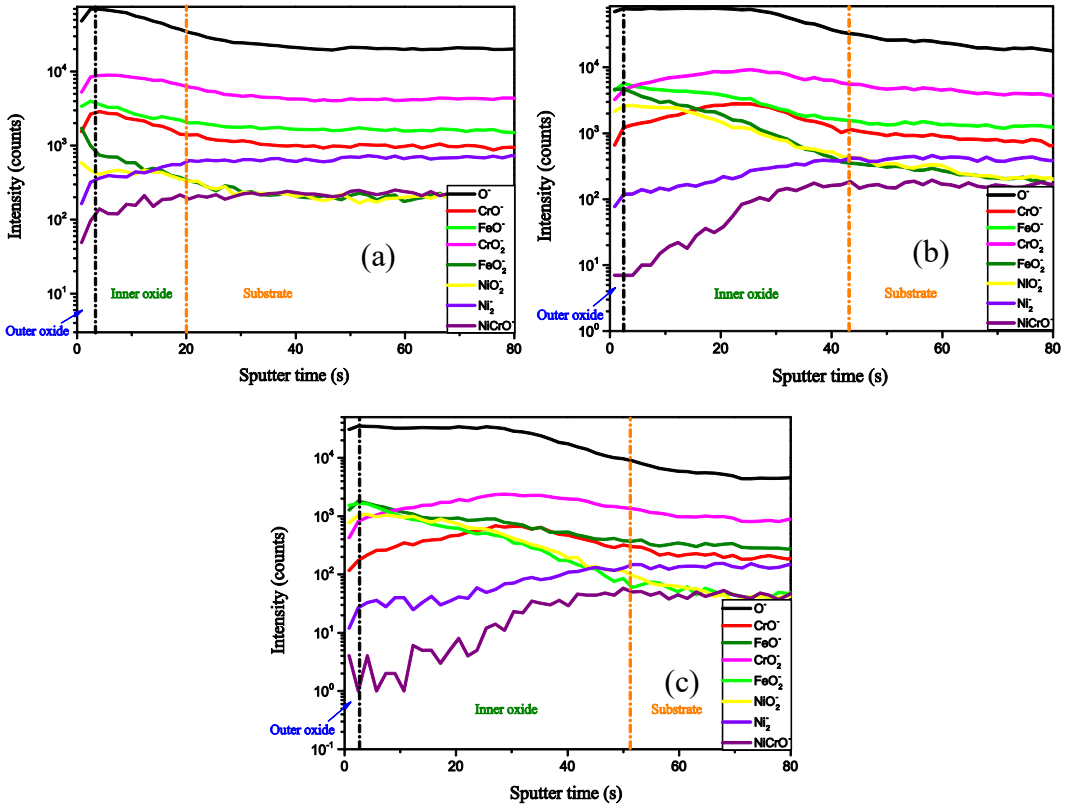

Fig. 2. ToF-SIMS profiles [Bi^+ 1.2 pA, 30×30 μm^2, Cs^+ 20 nA, 500 eV, 150×150 μm^2] obtained on the

polycrystalline Ni alloy after oxidation at 350℃ for 1 min (a), 15 min (b) and 3 h (c).

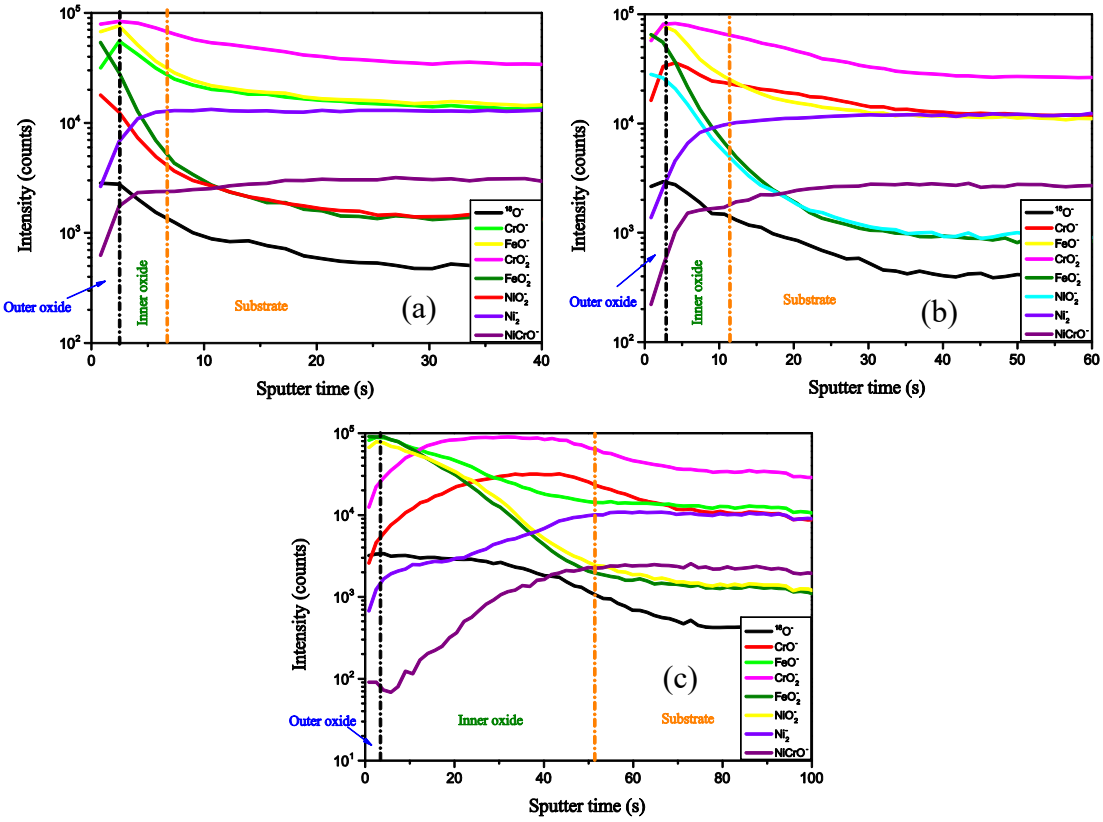

Fig. 3. ToF-SIMS profiles [Bi^+ 1.2 pA, 30×30 μm^2, Cs^+ 20 nA, 500 eV, 150×150 μm^2] obtained on the monocrystalline Ni alloy oriented (111) after oxidation at 350℃ for 5 min (a), 30 min (b) and 4 h 30 min (c).

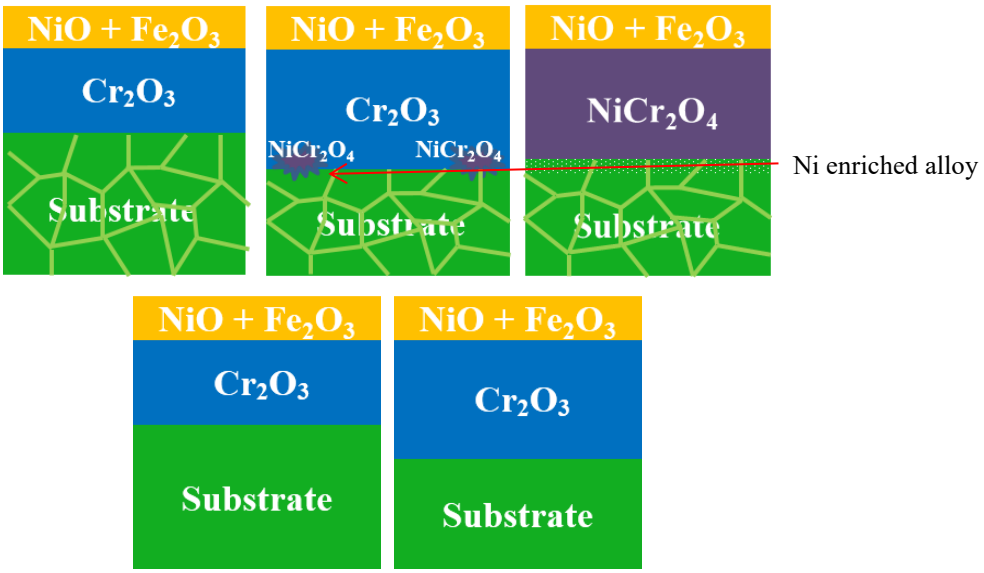

Fig. 4. Scheme of the evolution of the oxide composition of polycrystalline (first row) and monocrystalline (second row) Ni alloys.

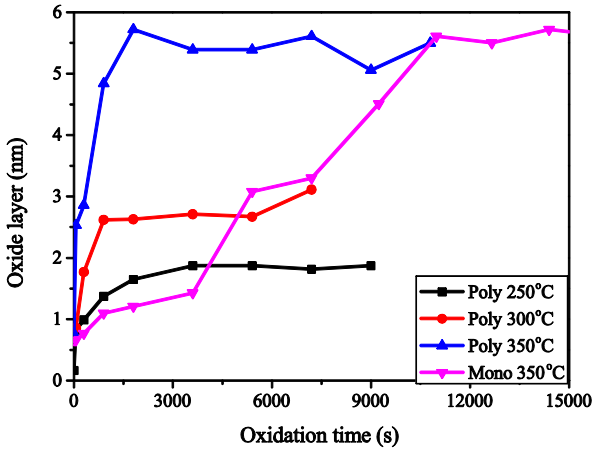

Fig. 5. Oxidation kinetics for poly and monocrystalline Ni alloys at different temperatures (Oxygen pressure = 1.2×10^{-6} mbar).

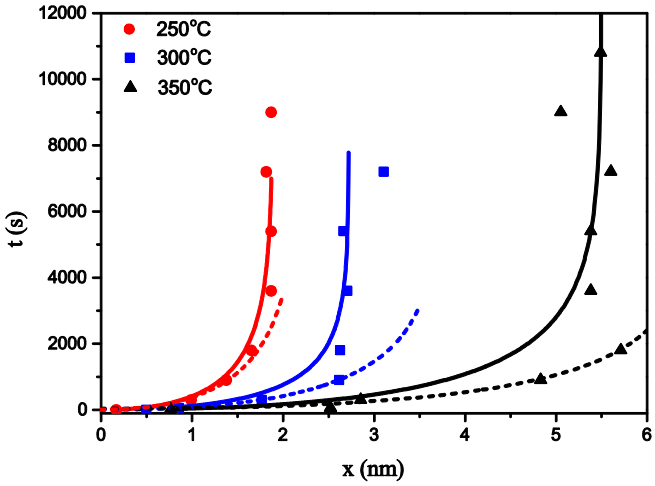

Fig. 6. Fit of the oxidation kinetics for three oxidation temperatures (solid lines, oxygen pressure = 1.2×10^{-6} mbar).

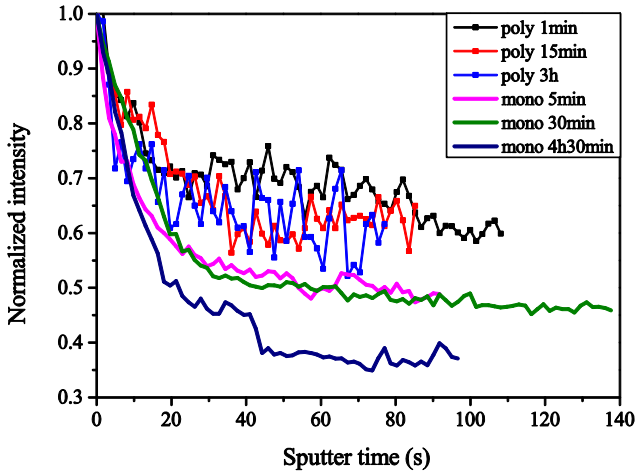

Fig. 7. Normalized profiles of the CrO^- signal after the M/O interface for the polycrystalline and monocrystalline alloys oxidized at 350℃ (Oxygen pressure = 1.2×10^{-6} mbar).

Table 1

Oxidation kinetics of the polycrystalline Ni alloy for three oxidation temperatures.

T(℃)	fit	k_p ($nm^2.s^{-1}$)	k_v ($nm.s^{-1}$)	D ($cm^2.s^{-1}$)
250	Solid line	1.9×10^{-3}	1.0×10^{-3}	/
	Dashed line	2.0×10^{-3}	9×10^{-4}	1.0×10^{-17}
300	Solid line	5.9×10^{-3}	2.2×10^{-3}	/
	Dashed line	7.8×10^{-3}	2.1×10^{-3}	3.9×10^{-17}
350	Solid line	1.6×10^{-2}	2.9×10^{-3}	/
	Dashed line	2.9×10^{-2}	4.4×10^{-3}	1.5×10^{-16}